REVIEW ARTICLE

Update on Brain Tumor Imaging: From Anatomy to Physiology

S. Cha

The role of neuroimaging in patients with brain tumors is no longer simply to evaluate structural abnormality and identify tumor-related complications. By transitioning from a purely anatomy-based discipline to one that incorporates functional, hemodynamic, metabolic, cellular, and cytoarchitectural alterations, the current state of neuroimaging has evolved into a comprehensive diagnostic tool that allows characterization of morphologic as well as biologic alterations to diagnose and grade brain tumors and to monitor and assess treatment response and patient prognosis. To treat patients with brain tumors without the use of neuroimaging is impossible to imagine. The intense efforts to develop, validate, and clinically implement quantitative, biology-driven neuroimaging methodologies are of utmost importance in selecting and developing appropriate therapy, detecting early treatment failure, and providing accurate and clinically relevant biologic end points for high-risk, but potentially high-reward, tumor-specific therapies tailored to the unique biology of an individual brain tumor.

This article provides an overview of the current state of neuroimaging of brain tumors and discusses 3 types of physiology-based MR imaging methods, namely, diffusion-weighted imaging (DWI), proton MR spectroscopy (^{1}H-MR spectroscopy), and perfusion-weighted imaging. These methods have played a pivotal role in the transition of clinical MR imaging from a purely morphology-based discipline to one that combines structure with function. Detailed discussion on the underlying MR physics behind each method is beyond the scope of this review, and the physics will be discussed only briefly when relevant. The review will focus instead on the clinical application of these methods as they relate to patients with brain tumors and will expand on exciting research applications of newer technologies.

Unique Features of Brain Tumors

The brain is the organ that defines a human being as a self and differentiates the human from other animals by its ability to perform higher-order cognitive functions that enable thoughts, emotions, memories, and dreams. Unlike any other organ in the human body, the brain has a multilayered protection and defense mechanism that keeps foreign substance away and maintains a delicate system that ensures a homeostatic milieu. The rigid skull is an obvious structural defense against physical trauma, but there are other structural and functional barriers, such as the blood-brain barrier (BBB), and autoregulation mechanisms that strive to maintain homeostasis of the brain environment.[1] These structural and functional barriers create a uniquely challenging environment for brain tumor cells to grow and prosper. As in diffuse gliomas, the most common type of primary brain tumor, the predominant growth pattern becomes infiltrative rather than expansile within the functioning brain parenchyma and along the inside of the BBB until late in tumor growth. Complete surgical resection therefore may be technically possible but usually is not performed because of unacceptable neurologic morbidity and permanent brain injury.

No matter what type of histologic features or genetic origin, brain tumors all have in common that they are confined by the inherent barriers of the brain and must learn to survive and thrive in the environment of both physical and functional barriers of the brain. The BBB is unique and one of the most important barriers of the brain, but there are others such as the structural barriers created by myelin sheath and axonal composition of white matter and cell nuclei of gray matter. These barriers and cytoarchitecture of the brain also offer opportunities for MR imaging to exploit unique changes of proton motion, metabolic activity, and hemodynamics created by the presence of tumor.

Classification of Brain Tumors

In 2000, the World Health Organization (WHO) revised the classification of neoplasms affecting the central nervous system, based on a century-old premise that each type of tumor originated from one specific cell type.[2] Purely on the basis of histologic features, this classification system relies almost entirely on visual assessment of the microscopic appearance of the tumor specimen, which raises the concern for subjectivity and interobserver variability. Moreover, the classification system does not take into consideration other important factors such as anatomic location and size of the tumor, both of which will determine surgical accessibility and degree of resectability.

Despite its shortcomings, the WHO classification scheme of brain tumors remains the primary basis for guiding therapy and assessing overall prognosis in patients with brain tumor. The classification system also forms the basis for scientific study in brain tumor research, as well as the clinical understanding of tumor biology, clinical response, and patient prognosis. Although most malignant brain tumors are uniformly fatal, rare but distinct instances do occur in which tumors respond to therapy and cure is achieved. The current WHO classification, however, falls short of predicting therapeutic response of each individual tumor within the same histologic grade and cannot provide precise guidance of therapy, especially those targeting specific molecular or genetic pathways of tumor genesis. Clearly, a need exists for improvement in the brain tumor classification scheme to one that can guide therapy and assess early treatment response and is clinically significant in terms of providing clinical end points and outcome

From the Department of Radiology and Neurological Surgery, University of California, San Francisco, San Francisco, Calif.

Supported by Grant NS045013-03.

Address correspondence to Soonmee Cha, MD, Department of Radiology and Neurological Surgery, University of California, San Francisco, 505 Parnassus Ave, Room L-358, San Francisco, CA 94143-0628.

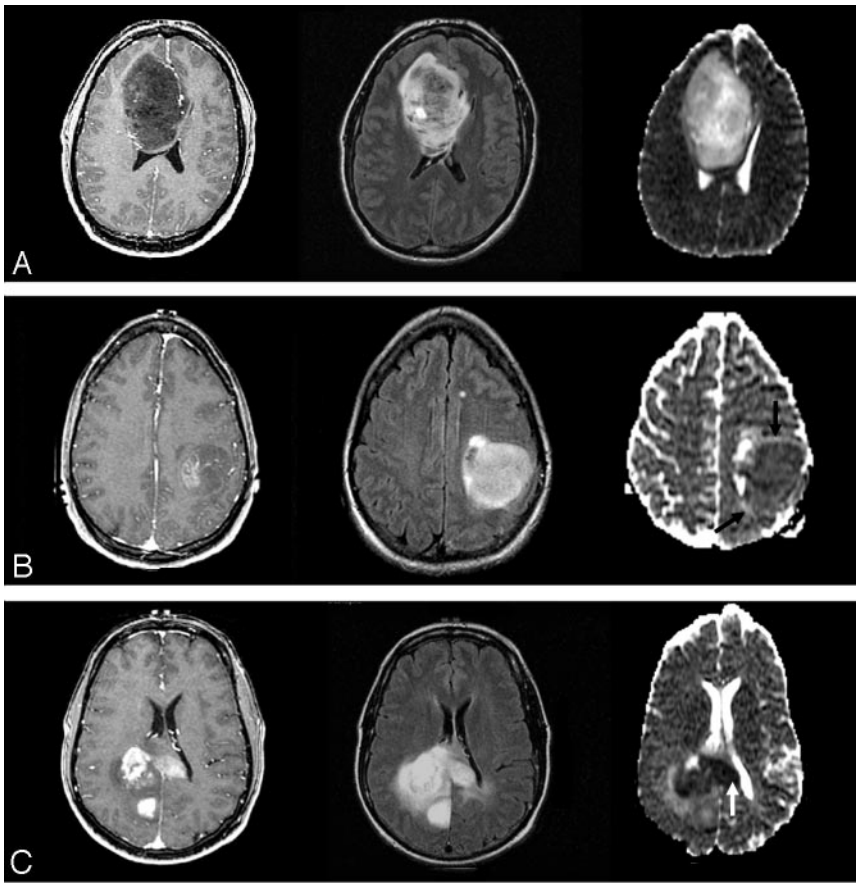

Fig 1. ADC and astrocytoma grade. WHO grade II (*top row*), grade III (*middle row*), and grade IV (*bottom row*) astrocytomas. Axial postcontrast T1-weighted images (*left column*), FLAIR images (*middle column*), and ADC maps (*right column*) demonstrate typical examples of 3 different grades of astrocytoma. With increasing tumor grade, the tumor ADC value of grade III astrocytoma is lower (*black arrows*) than that of grade II and the grade IV astrocytoma has the lowest (*white arrow*).

measures. It is unlikely that, on the basis of histologic classification alone, the grading of brain tumors will provide meaningful end points for therapeutic trials. To that end, surrogate or biologic tumor markers derived from neuroimaging hold much promise to fill that role by potentially providing novel information on biologic differences between 2 tumors of the same type and grade that respond drastically differently to therapy.

Physiology-Based MR Imaging

DWI. Four important clinical applications of DWI in brain tumors have been to assess tumor grade and cellularity, postoperative injury, peritumoral edema, and integrity of white matter tracts.

Apparent Diffusion Coefficient and Glioma Grade. The grade of brain tumor is pivotal in the treatment decision and assessment of prognosis. The revised WHO classification subdivides gliomas into 4 grades (I–IV) based on specific histologic features of tumor such as cellularity, nuclear atypia, mitotic activity, pleomorphism, vascular hyperplasia, and necrosis. Grade I gliomas comprise a unique group of gliomas—pilocytic astrocytoma, pleomorphic xanthoastrocytoma, subependymal giant cell astrocytoma—which all share a relatively benign biology and indolent clinical course. The remaining diffuse gliomas are subdivided into grades II–IV, which is the basis for our understanding of tumor biology and clinical outcome. Of the histologic features for glioma grading, cellularity has been the target of quantitative assessment with DWI. The rationale of using DWI to quantify cellularity is based on the premise that water diffusivity within the extracellular compartment is inversely related to the content and attenuation of the constituents of the intracellular space. The higher the tumor cellularity (and hence the greater volume of intracellular space), the lower the apparent diffusion coefficient (ADC) because of decreased water diffusivity caused by a relative reduction in extracellular space for the proton to move about. Hence, the higher the glioma's grade, the lower mean tumor ADC values (Fig 1). Several reports have shown that glioma grade correlates inversely with minimum ADC, likely on the basis of increasing tumor cellularity with grade.[3-6] Although the initial reports on the correlation between minimum ADC and glioma grade have shown promise, the role of DWI in the preoperative assessment of glioma grade is clinically insignificant and remains investigational, because of substantial overlap in ADC values among different grades of glioma. The limited role of ADC in glioma grading is less likely because of the limitation of ADC as a quantitative biomarker of cellularity but more likely because of inherent and quite remarkable tissue heterogeneity associated with gliomas across different grades, within the same grade, and even within a single given tumor. It is widely known that a given individual glioma, usually of high grade, often contains a continuum of histologic features of grades II–IV, and tumor grading is dependent entirely on the site of tumor biopsy or resection and

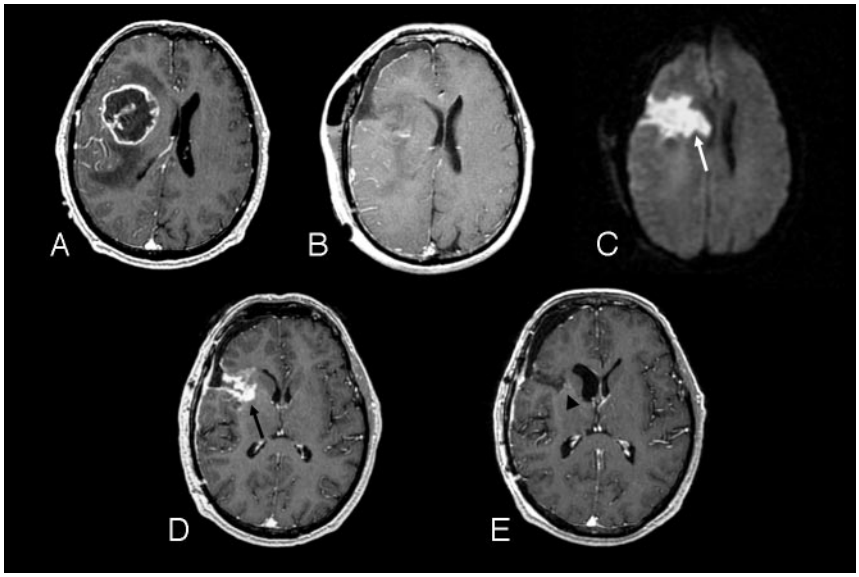

Fig 2. A 51-year-old man with right frontal glioblastoma multiforme.

A, Preoperative axial postcontrast T1-weighted image shows a centrally necrotic, peripherally enhancing right frontal lobe mass compressing the adjacent lateral ventricle.

B, Immediately postoperative axial postcontrast T1-weighted image confirms gross total resection of the enhancing portion of the mass.

C, Immediately postoperative axial diffusion-weighted image demonstrates a wedge-shaped area of abnormal reduced diffusion (*white arrow*) within the surgical bed.

D, One-month postoperative axial postcontrast T1-weighted image reveals irregular area (*black arrow*) of abnormal contrast enhancement within the margins of the surgical bed simulating the appearance of a recurrent tumor.

E, Two-month postoperative axial postcontrast T1-weighted image shows complete resolution of the abnormal contrast enhancement and a gliotic cavity (*arrowhead*).

thus subject to sampling error or undersampling. The range of ADC values within a given glioma therefore can vary markedly, and a measurement derived from a region of interest will underscore the spectrum of heterogeneity in glioma cellularity.

ADC values have also been correlated with cellularity of nonglial brain tumors. When compared with gliomas, lymphomas were shown to have lower ADC, likely because of their higher cellularity.[7] In a small sample of meningiomas, malignant or atypical meningiomas were found to have lower ADC values when compared with typical meningiomas.[8] Although the underlying physics of reduced diffusion in certain brain tumors is far more complex than that due to increased cellularity, minimum ADC seems to correlate well with brain tumors of higher cellularity. It should be noted that none of these studies actually performed ADC-guided tissue biopsy to confirm the correlation between minimum ADC and tumor cellularity.

DWI and Postoperative Injury

Reduced diffusion abnormality is not synonymous with acute cytotoxic edema, because it can be seen in numerous intracranial disease processes that do not involve cytotoxic edema. Any process that results in acute intracellular swelling and subsequent decrease in the surrounding extracellular space can lead to reduced proton diffusion in the brain. After brain tumor resection, acute cellular damage is likely to occur for a variety of reasons such as direct surgical trauma, retraction and vascular injury, and devascularization of tumor. A recent report suggests that the occurrence of abnormal reduced diffusion in and around as well as remote from the resection bed immediately after surgery for brain tumor resection is not uncommon.[9] The important clinical implication here is not so much in the observation of areas of reduced diffusion after surgery as the knowledge of the evolution of these abnormalities in the follow-up phase as the patient undergoes adjuvant radiation therapy and/or chemotherapy. Similar to the evolution of reduced diffusion in the setting of acute infarct, the areas of immediate postoperative diffusion abnormality invariably undergo a phase of contrast enhancement on routine anatomic images that can be easily misinterpreted as tumor recurrence. In a recent study,[9] regions of reduced diffusion after glioma surgery showed contrast enhancement on a follow-up study that simulated the appearance of recurrent tumor. These areas of enhancement invariably evolved into encephalomalacia or gliotic cavity on long-term follow-up studies, as one would expect in a region of permanent brain injury. After surgery, it is important to recognize diffusion-related contrast enhancement in gliomas, which can be confused with the appearance of recurrent tumor and interpreted erroneously as an early treatment failure, prompting aggressive therapy with high potential toxicity and questionable efficacy (Fig 2). A new area of contrast enhancement observed on postcontrast T1-weighted images after glioma surgery should be interpreted in the context of the immediate postoperative DWI, a sequence that is essential and should be a part of any routine brain tumor imaging protocol.

ADC and Peritumoral Edema: Vasogenic versus Infiltrative

The modern-day concept of cerebral edema remains largely based on the theory of Klatzo, who in 1967 proposed 2 fundamentally different types of edema, cytotoxic and vasogenic.[10] In cytotoxic edema, the chief mechanism is related to intracellular swelling due to sodium influx after energy pump failure at the cell membrane level. The net result of cytotoxic edema is

marked decrease in extracellular space and, hence, marked reduction in ADC measurement ($<0.5 \times 10^{-3}$ mm^2/s) seen in the setting of acute cerebral infarct. In vasogenic edema, however, there is increase in extracellular space volume, because of disturbance of vascular permeability, which enables the indiscriminate escape of plasma fluid and protein. Unlike cytotoxic edema, vasogenic edema implies reactive changes rather than permanent cellular damage and, hence, is reversible. In brain tumors, peritumoral edema is largely based on imaging definition of different components of tumor in relation to the presence or absence of contrast enhancement after the administration of intravenous contrast agent such as gadopentetate dimeglumine (Gd-DTPA) for MR imaging. In general, the nonenhancing area of abnormality surrounding the enhancing tumor core is referred to as peritumoral edema. In metastatic brain tumors or noninfiltrative primary tumors such as meningiomas, the peritumoral edema is synonymous with vasogenic edema, where there is increased extracellular water due to leakage of plasma fluid from altered tumor capillaries but no tumor cells are present. In gliomas, however, the peritumoral edema is better referred to as infiltrative edema, because it represents both vasogenic edema and infiltrating tumor cells that are behind the BBB and usually invading along the white matter tracts.

Imaging-based localization of scattered and random areas of tumor infiltration within the peritumoral edema in gliomas is a daunting, if not impossible, task because infiltrated tumor cells are barely identifiable even at histologic evaluation at a microscopic level, a resolution that is far beyond what anatomic MR imaging can provide. Differentiation between vasogenic and infiltrative edema has been attempted with DWI on the basis of the premise that water diffusivity is facilitated to a greater degree in vasogenic than in infiltrative edema because of a lack of intervening tumor cells in the former. The real challenge, however, is to localize tumor-infiltrated regions among the area of vasogenic edema so that potential therapy can be directed to these sites without subjecting unnecessary toxicity on the entire peritumoral edema, most of which is vasogenic in nature. Several reports have shown that ADC values are not helpful in differentiating tumor and tumor-related brain edema.[11,12] Although there was one report[13] showing reported statistically significantly different ADC values between the 2 types of edema in 2 different tumor types (gliomas vs metastatic tumors), it is unlikely that ADC alone will be able to discriminate pure white matter water as in vasogenic edema from brain water with scattered foci of microscopic and isolated tumor cells as in infiltrative edema because of the inherent limitation of spatial resolution of DWI.

Another application of DWI in brain tumors is the use of fractional anisotropy (FA) maps derived from diffusion tensor imaging (DTI) to determine the integrity of white matter tracts in the vicinity of a brain tumor. Several different patterns of FA maps were described in a recent report proposing to differentiate white matter tracts that are displaced or distorted but intact from those that are invaded or destroyed by the adjacent tumor.[14] Although there is lack of direct histologic correlation between FA maps and the status of white matter tracts near brain tumor in the literature, a variation of FA matrices such as the tumor infiltration index[15] or fiber attenuation index[16] may provide more specific information on the status of peritumoral edema in brain tumors. The biologic correlates for the DTI-derived matrices, however, remain unclear and await much-needed histologic validation.

Diffusion Tensor Imaging and White Matter Tractography

Diffusion tensor imaging (DTI) is a rapidly growing area of research in technical optimization and image processing, as well as clinical application in a variety of intracranial disorders. DTI is distinguished from DWI by its sensitivity to anisotropic or directionally dependent diffusion and provides unique information on 3D diffusivity, which is characterized by 3 eigenvectors (direction) and 3 eigenvalues (magnitude). In humans, brain DTI provides a 3D depiction of white matter connectivity that allows unprecedented opportunity to study brain cytoarchitecture at a microscopic level. The term "tensor" is a mathematic construct adopted from physics and engineering to describe tension forces in solid bodies with an array of 3D vectors. In DTI, tensor is made up of a matrix of numbers derived from diffusion measurements in at least 6 independent diffusion-encoding directions to calculate orientation-dependent diffusion in all spatial directions for each image voxel. The anisotropic diffusion in the brain is largely attributed to 2 unique cytoarchitectural compositions of the brain: myelin and axons. The lipid bilayer of myelin sheath creates a unique microsopic diffusion barrier that results in different degrees of diffusion along different planes.[17] Myelin alone, however, cannot be responsible for anisotropic diffusion, because nonmyelinated nerves have been shown to demonstrate striking diffusion anisotropy.[18] The attenuation and packing of axons and the subcomponents of axons such as the micro- and neurofilaments, microtubules, and membranes also contribute significantly to the anisotropic diffusion. Although the biologic basis of diffusion anisotropy is not yet completely understood, the differential degree of water diffusivity that is maximal parallel to and minimal perpendicular to the long axes of collimated axonal bundles and myelin sheath create a unique situation to measure and tract fiber orientation, especially in large white matter tracts such as the corticospinal tract.

In brain tumors, DTI tractography has had a tremendous impact on intraoperative guidance in tumor resection.[19] DTI tractography maps of desired white matter tracts can be overlaid onto high-resolution anatomic images and provide information on alterations in fiber tract directionality and integrity due to neighboring brain tumor (Fig 3). DTI tractography of the corticospinal tract has gained popularity among neurosurgical colleagues as a noninvasive guide to avoid injuring the corticospinal tract during tumor resection.

Proton MR Spectroscopic Imaging

MR Spectroscopy and Glioma Grading. The clinical value of preoperative glioma grading based on metabolite ratios derived from ^{1}H-MR spectroscopy remains investigational despite several published reports on high diagnostic accuracy of ^{1}H-MR spectroscopy. Currently, the role of MR spectroscopy in glioma grading in the clinical preoperative setting, especially in replacing surgical biopsy, has not been proved accurate enough to replace tissue diagnosis and grading. Several large case series have reported that ^{1}H-MR spectroscopy was very accurate in the differentiation of high- and low-grade

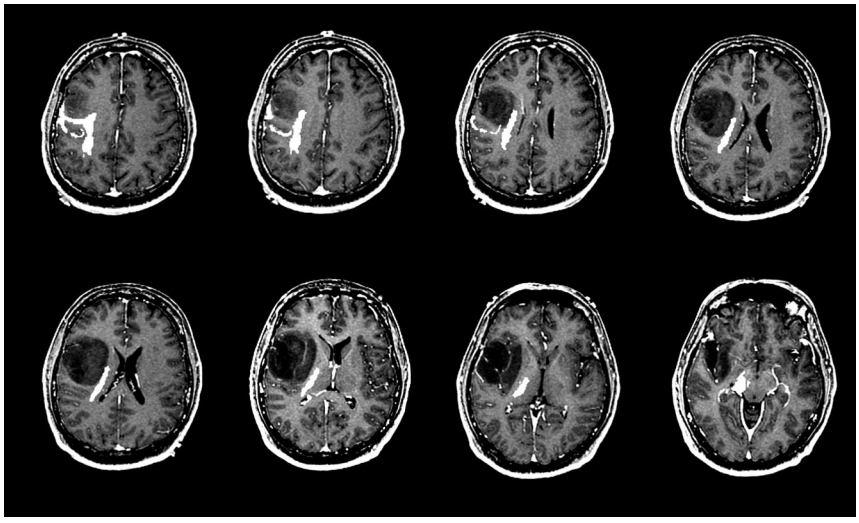

Fig 3. A 37-year-old man with right frontal low-grade astrocytoma. A series of axial postcontrast T1-weighted images of the brain demonstrate a nonenhancing right frontal insular mass. The diffusion tensor tractogram, which has been coregistered and overlaid onto the contrast-enhanced T1-weighted images, demonstrates corticospinal tract (*white marks*) that is displaced but not invaded by the tumor.

gliomas,[20-23] by using both the long and/or short echo-time studies, though there was diminished diagnostic accuracy in the differentiation between grade III and grade IV gliomas.[24] None of these studies, however, compared the accuracy of ^{1}H-MR spectroscopy in glioma grading with contrast-enhanced anatomic MR imaging, which should be considered the reference standard.

MR Spectroscopy and Tumor versus Therapy-Related Changes. Imaging assessment of brain tumor after therapy is particularly challenging for neuroradiologists and neuro-oncologists, because of the nonspecificity of anatomic imaging. Areas of contrast enhancement on enhanced T1-weighted images after glioma therapy often contain both residual or recurrent tumor and therapy-related changes, and precise localization and separation of the 2 regions within a given tumor has proved difficult. Nonetheless, differentiating tumor and therapy-related necrosis by using imaging continues to be the subject of intense research objectives throughout the world and still remains the elusive "Holy Grail" of brain tumor imaging after therapy. Aside from imaging, the extreme histologic and geographic heterogeneity of gliomas before and after therapy poses another challenge in separating tumor and necrosis even on histopathologic evaluation.

^{1}H-MR spectroscopy has been used clinically to differentiate tumor- and therapy-related changes mostly in irradiated gliomas in several published reports.[25-27] These studies contain relatively small samples (all $<$45 patients), but have shown that abnormal increase in choline peak $>$50% of the contralateral brain or choline-to-creatine ratio $>$2 had moderate to high sensitivity (64%–95%) and high specificity (82%–100%) for identifying active tumor. Lack of studies with larger samples, however, makes the results from small case series difficult to extrapolate and apply clinically in a wider context in an attempt to bypass surgical confirmation.

Lactate-Edited ^{1}H-MR Spectroscopy

Glioblastoma multiforme, the most common type of primary glioma, has extensive areas of hypoxia and necrosis.[28] An increasing body of evidence suggests that hypoxia in glioma is a powerful promoter of tumor angiogenesis and invasion through its upregulation of target genes critical for these functions.[29-32] Hypoxia-driven angiogenesis sets up a vicious cycle of production of immature, abnormal microvasculature that cannot function properly and thus results in more tumor hypoxia, ultimately resulting in necrosis.

Lactate is the end-product of the nonoxidative glycolysis. Therefore, its presence may be correlated with poor oxygenation level, or hypoxia, in the tumor tissue.[33] The presence of mobile lipids has been correlated with the formation of necrosis where cellular death results in membrane breakdown.[34] In gliomas, mobile lipids are observed mostly in high-grade tumors, particularly in gliobastoma multiforme,[35] because of its characteristic pseudopalisading necrosis, whereas the correlation of the presence of lactate with glioma grade remains uncertain.[36-38] In standard ^{1}H-MR spectroscopy acquisition, the peaks of lactate and mobile lipids overlap within the region from 0.9 to 1.3 parts per million (ppm). Because of this proximity of resonance on ^{1}H-MR spectra, lactate and lipids are often treated as a single metabolite, though each represents vastly different tumor biology and tissue viability. The regions of lactate most likely represent areas of hypoxic but viable tumor, whereas the regions of mobile lipid represent necrotic nonviable tissue. The separate detection and quantification of the 2 metabolites are therefore important in studying the relationship between hypoxia and necrosis within a brain tumor.

Spectral editing is necessary to detect the intensity of lactate and mobile lipid metabolites separately and reliably at ^{1}H-MR spectroscopy. The methods based on J-difference modulation allow for the distinction between coupled and uncoupled spins and achieve full sensitivity of the lactate doublet[39] at 1.2 ppm. This class of techniques, however, needs 2 acquisition cycles per phase-encoding step, and the total acquisition time is generally too long for routine clinical applications. Reduced k-space sampling techniques such as the ellipsoidal k-space sampling method can reduce the acquisition time so that clinical imaging is practical for studies of patients with brain tumor.

Clinical application of lactate-edited ^{1}H-MR spectroscopy

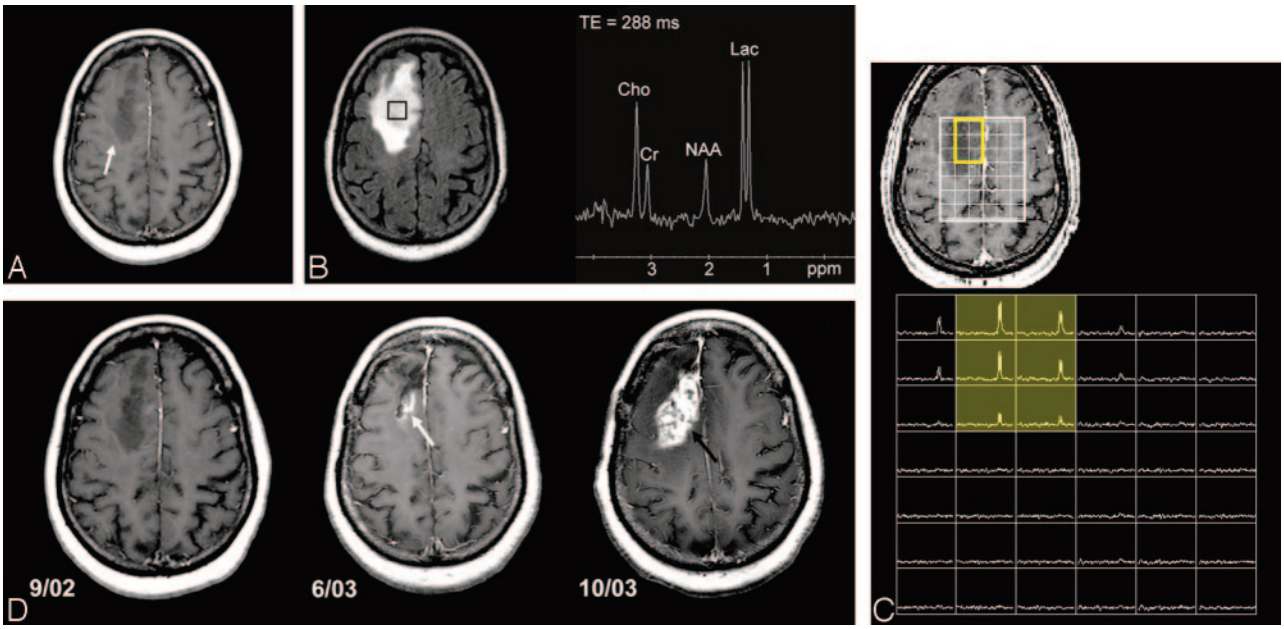

Fig 4. A 59-year-old woman with right superior frontal mass initially diagnosed as low-grade astrocytoma.

A, Axial postcontrast T1-weighted image shows an ill-defined nonenhancing mass within the right superior frontal lobe.

B, Axial FLAIR image demonstrates homogeneous T2 prolongation within the mass and a single-voxel proton-spectroscopic imaging within the center of the mass reveals a marked increase in lactate (Lac) and choine (Cho) metabolites and a decrease in *N*-acetylaspartate (NAA) metabolite.

C, 3D, lactate-edited, proton spectroscopic image of the same tumor location confirms the presence of lactate metabolite within the tumor. Re-evaluation of the tissue specimen revealed a few mitotic figures and vascular hyperplasia, and the tumor was upgraded to anaplastic astrocytoma.

D, Serial axial postcontrast T1-weighted images during 1-year period show emergence of subtle enhancement at the posterior surgical margin at 9-month follow-up (*white arrow*), which rapidly progresses into an aggressive grade IV astrocytoma (*black arrow*).

has shown a promising role for lactate and lipid metabolites in further differentiating glioma grades, especially between high- and low-grade gliomas (Fig 4). A recent report suggests that mobile lipid is present almost exclusively in high-grade gliomas but rarely, if at all, in low-grade gliomas and that lactate is seen in both grades of gliomas. More interestingly, the regions of high lactate or lipid metabolite peaks were seen in close proximity, if not identical, to the areas of maximal tumor blood volume abnormality assessed by dynamic susceptibility-weighted contrast-enhanced (DSC) MR imaging.[40] It is widely known from the neuropathology literature that hypoxia is one of the most potent stimulators of tumor angiogenesis in gliomas. Intense research in this field has revealed the complexity of glioma angiogenesis and the delicate balance and interplay between anti- and proangiogenic influences, including tumor hypoxia.[32] The previous report[40] on ^{1}H-MR spectroscopy and DSC MR imaging seems to suggest that there is a spatial, if not also temporal, relationship between tumor hypoxia and tumor angiogenesis. It remains to be seen, however, whether lactate from ^{1}H-MR spectroscopy correlates directly with histologic assessment of tumor hypoxia, such as antibody staining of hypoxia-inducible factor. Results of a recent preliminary study[41] suggest that lactate metabolite may be a surrogate marker of radioresistance in gliomas undergoing radiation therapy. Although lack of sufficient data underscores using lactate metabolite derived from ^{1}H-MR spectroscopy as a reliable biomarker of tumor hypoxia or radioresistance, robust separation of lactate and lipid metabolites in gliomas is an important step toward establishing the biologic significance of each metabolite.

MR Spectroscopy Summary

^{1}H-MR spectroscopy is a powerful noninvasive imaging technique that offers unique metabolic information on brain tumor biology that is not available from anatomic imaging. ^{1}H-MR spectroscopy has shown a promising role in grading low- and high-grade gliomas and also in differentiating active tumor from therapy-related necrosis. Several technical issues face ^{1}H-MR spectroscopy, however, including variable and nonstandardized pulse sequences and the lack of standardized quantitation methods and diagnostic threshold for metabolite concentration that can be used in multi-institutional and multiple vendor platforms. Other issues include incomplete coverage of tumor tissue because of the limitation of spectral volume size and artifacts from bone and scalp tissues. Despite these challenges, ^{1}H-MR spectroscopy will continue to play an important role in providing noninvasive metabolic information on brain tumors that forms the basis for intense scientific research in technical refinements and remains a part of the clinical diagnostic armamentarium to improve brain tumor diagnosis.

Perfusion MR Imaging

In brain tumors, perfusion MR imaging proposes to measure the degree of tumor angiogenesis and capillary permeability, both of which are important biologic markers of malignancy, grading, and prognosis, particularly in gliomas. Brain tumor vasculature plays critical roles not only in supplying nutrients and oxygen to tumor cells but also in providing a roadmap for tumor infiltration and complex feedback loop with tumor hypoxia and necrosis.[42-44] It is of utmost importance to un-

derstand the complex biology of brain tumor angiogenesis to gain insight into the development of malignancy and strategies to combat tumor growth.[45] To that end, various perfusion MR imaging methods strive to provide noninvasive and robust surrogate markers of tumor angiogenesis and capillary permeability. The following sections focus on the 2 most widely used contrast-enhanced MR imaging methods—DSC and dynamic contrast-enhanced (DCE) perfusion MR imaging—to study and quantify brain tumor vasculature.

DSC MR Imaging

The most robust and widely used quantitative variable derived from DSC imaging is the relative cerebral blood volume (rCBV). It has been shown by Zierler[46] that, in the absence of recirculation and contrast material leakage, CBV is proportional to the area under the contrast agent concentration-time curve. From the susceptibility signal intensity–time curve, Gd-DTPA concentration, which is proportional to the change in relaxation rate ([$\Delta R2^*$] ie, the change in the reciprocal of $T2^*$), can be calculated from the signal intensity by using the following equation[47]:

$$1) \qquad \Delta R2^* = \frac{-\ln(S(t)/S_0)}{TE}$$

where $S(t)$ is the pixel signal intensity at time t, S_0 is the precontrast signal intensity, and TE is the echo time. This equation is only valid if T1 enhancement associated with BBB disruption has a negligible effect on signal intensity, which is ensured by using either long TRs, low flip angles, or a combination of the 2 to reduce saturation.

In general, the assumptions of negligible recirculation and contrast material leakage are violated. The effects of this can be reduced by fitting a gamma-variate function to the measured $\Delta R2^*$ curve.[48] The gamma-variate function approximates the curve that would have been obtained without recirculation or leakage. CBV can then be estimated from the area under this fitted curve rather than the original data. In our experience, however, the gamma variate fit is unstable: small variations in the initial parameter estimates give wide variations in the results. This instability occurs even with data averaged over regions of interest in areas of high perfusion and appears to be inherent to the procedure. In practice, satisfactory fits can often be found only by repeating the procedure with multiple different initial estimates until a set is found that causes the fitting algorithm to converge. This approach can be applied to fit time-concentration curves from multiple regions of interest, because each fit takes very little time but is not suited for pixel-by-pixel calculations of CBV maps. To obtain CBV maps, alternative corrections for leakage are therefore needed. The simplest method is to estimate the end of the bolus and calculate the area under the bolus alone. This will, however, result in a systematic overestimation of CBV in areas where the BBB is damaged. Alternatively, having estimated the beginning and end of the bolus, a baseline can be subtracted from under the curve. The area under the corrected contrast agent concentration-time curve is *proportional* to the CBV and does not yield an absolute measurement. It is therefore necessary to express the measurement relative to a standard reference, usually contralateral white matter.

Numerous studies have attempted to correct for the under- or overestimation of rCBV measurements from DSC imaging in regions of microvascular leakage and to derive new parameters to more accurately characterize endothelial permeability.[49-56] These include methods such as preinjecting a small amount of Gd-DTPA to temporarily saturate the tissue T1, dual-echo pulse sequences, baseline subtraction, and model-based permeability compensation methods. Each has its own strength and weakness, and none is considered the reference standard method to correct for leakage factor.

A recent study[57] showed that new quantitative variables other than CBV can be derived from DSC perfusion MR imaging without making the assumption of intact BBB. From the relaxivity signal intensity–time curve, the maximum susceptibility-weighted signal intensity change and the percentage signal intensity recovery at the end of the first pass can be easily calculated without complex modeling or a sophisticated leakage correction algorithm.

rCBV and Astrocytoma Grading. Gliomas are the most common primary tumors of the brain, with astrocytomas being the most common subtype. In astrocytomas, vascular morphology is a critical parameter in determining malignant potential and survival. Astrocytoma grading is important for determining both prognosis and therapy. Several studies[58-61] have shown a statistically strong correlation between tumor rCBV and astrocytoma grading, as well as conventional angiographic tumor vascularities. As the grade of fibrillary astrocytoma increases, the maximal tumor rCBV tends to increase (Fig 5). Astrocytoma grading by using rCBV, however, should be limited to fibrillary astrocytomas because other gliomas, most notably oligodendrogliomas, may have high rCBV regardless of grade (Fig 6).

Still unknown is what an elevated rCBV really represents histologically. To our knowledge, no report has been published on a direct correlation between rCBV and histologic features based on image-guided biopsy. This remains a challenging but necessary step in validating rCBV as a biomarker of tumor angiogenesis. Angiogenesis in brain tumors is as heterogeneous as the numerous types of histologic subtypes. For example, pilocytic astrocytomas, a common pediatric brain tumor and a WHO grade I astrocytoma, often demonstrate vascular hyperplasia that is composed of dilated vessels of fairly uniform morphology. Glioblastoma multiforme, a WHO grade IV astrocytoma, also frequently contains vascular hyperplasia that can be morphologically quite heterogeneous and includes classic glomeruloid vessels, simple endothelial hyperplasia, and delicate vasculature.

rCBV and Nonastrocytic Gliomas. As mentioned above, there are nonastrocytic gliomas that have high rCBV even in low-grade tumors. Oligodendrogliomas are well known for their delicate neoangiogenic vessels, the so-called chicken-wire vasculature, and demonstrate elevated rCBV, even in low-grade tumors, that can be as high as that of glioblastoma.[62] As shown in Fig 6, low-grade oligodendrogliomas tend to demonstrate high rCBV on DSC perfusion MR images and can, at times, be confused with malignant gliomas, even a glioblastoma. There are well-described conventional anatomic MR imaging features of oligodendrogliomas such as cortical involvement with frontal lobe predominance, intratumoral cysts, and susceptibility changes due to intratumoral

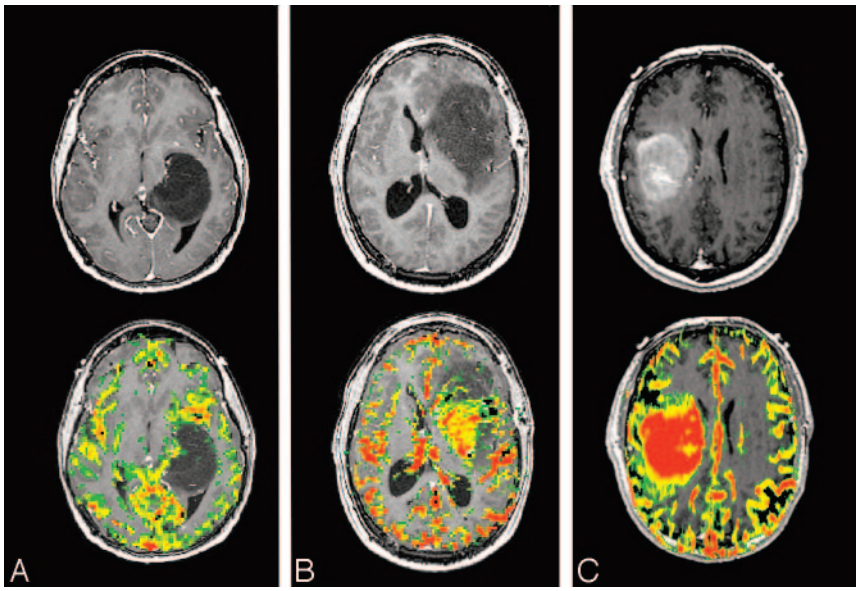

Fig 5. Relative cerebral blood volume (rCBV) maps of astrocytoma grade II, grade III, and grade IV (*left* to *right*).

Top row, Axial postcontrast T1-weighted images of grade II (*left*), grade III (*middle*), and grade IV (*right*) astrocytoma demonstrate definite contrast enhancement associated with only the grade IV tumor.

Bottom row, Axial rCBV color maps coregistered with axial postcontrast T1-weighted image show increasing tumor blood volume abnormality with increasing tumor grade.

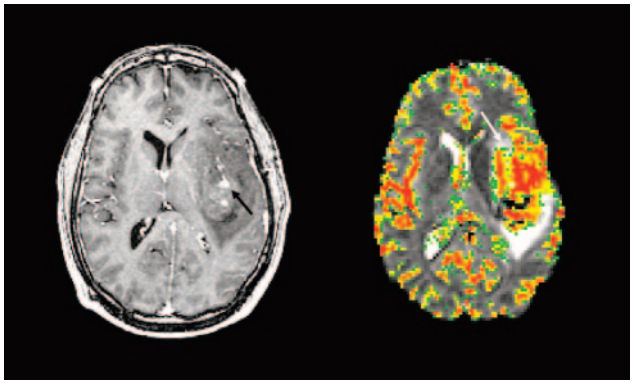

Fig 6. A 34-year-old man with left frontal grade II oligodendroglioma. Axial postcontrast T1-weighted image (*left*) shows a heterogeneous, mildly enhancing (*black arrow*) left frontal mass. Axial rCBV map at the same anatomic location demonstrates marked increased in tumor blood volume (*white arrow*).

calcification that, in conjunction with high rCBV, can help in preoperative diagnosis.

Choroid plexus tumors are gliomas that arise from the choroid plexus within the ventricular system of the brain. These are highly vascular tumors composed of capillaries derived from the choroid plexus, which does not contain a BBB. This results in highly leaky capillaries, which causes avid enhancement on T1-weighted images after administration of Gd-DTPA. On DSC perfusion MR images, choroid plexus tumors demonstrate marked leakage of Gd-DTPA at the start of the bolus phase, and the susceptibility-weighted signal intensity curve never returns toward baseline (Fig 7). Because there is no BBB, intravascular compartmentalization of Gd-DTPA is not possible due to almost simultaneous transition of the contrast agent from intravascular to interstitial space. The rCBV measurements of choroid plexus tumors tend to be markedly under- or overestimated because fitting of the $\Delta R2^*$ curve to yield area under the curve is unstable or unreliable.

rCBV and Brain Tumors Other Than Gliomas. Meningiomas are the second-most-common primary tumors of the brain. The most common meningiomas are biologically benign, WHO grade I tumors that are usually curative with complete surgical resection. The less common atypical meningiomas (WHO grade II) tend to be more clinically aggressive and are likely to recur even after complete resection. Regardless of grade, meningiomas are highly vascular tumors that usually derive blood supply from dural vessels of the external carotid artery, though pial supply is not uncommon. Results of a recent preliminary report[63] suggest that the type of vascular supply—dural or pial—may affect the characteristics of the susceptibility-weighted signal intensity–time curve where there was more profound contrast material leakage during the bolus phase for meningiomas that derive their blood supply from dural vessels compared with those tumors supplied by pial vessels (Fig 8). Although validity of this observation remains highly investigational, the concept of detecting the type of vascular supply to meningiomas by using DSC perfusion MR imaging has profound implications in selection of patients for preoperative embolization, which is limited to dural vessels, and surgical planning for pial-supplied meninigiomas, which tend to bleed more during surgery.

Primary cerebral lymphoma (PCL) is a highly malignant brain tumor, usually of B-cell lymphocyte origin. PCLs can mimic malignant primary gliomas (glioblastoma in particular), metastatic brain tumors, or even infection on anatomic MR images. Preoperative diagnosis of PCL is critical because, unlike primary gliomas, gross total resection of tumor in PCL is a relative contraindication and may, in fact, result in increased patient morbidity and mortality.[64] On DSC perfusion MR images, lymphomas tend to show elevated rCBV, but not to the degree as in glioblastoma. This is likely because florid angiogenesis is not a typical feature of PCL. Rather, PCL is well known for its angiocentric histologic feature where the lym-

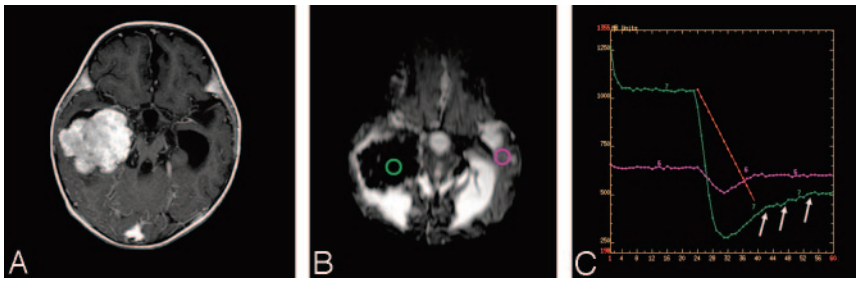

Fig 7. A 5-year-old girl with right lateral ventricle choroids plexus papilloma.

A, Axial postcontrast T1-weighted image shows an avidly enhancing, intraventricular mass.

B, Dynamic susceptibility-weighted contrast-enhanced image during the maximum bolus demonstrates marked signal intensity drop within the tumor because of increased tumor vascularity.

C, Susceptibility-weighted signal intensity time curves from regions of interest placed over the tumor (green) and the contralateral normal brain (pink) show marked difference in signal intensity recovery between the 2 regions. The tumor vasculature lacks blood-brain barrier and there is immediate and marked leakage of contrast agent during the bolus phase (*arrows*) and minimal return to the baseline.

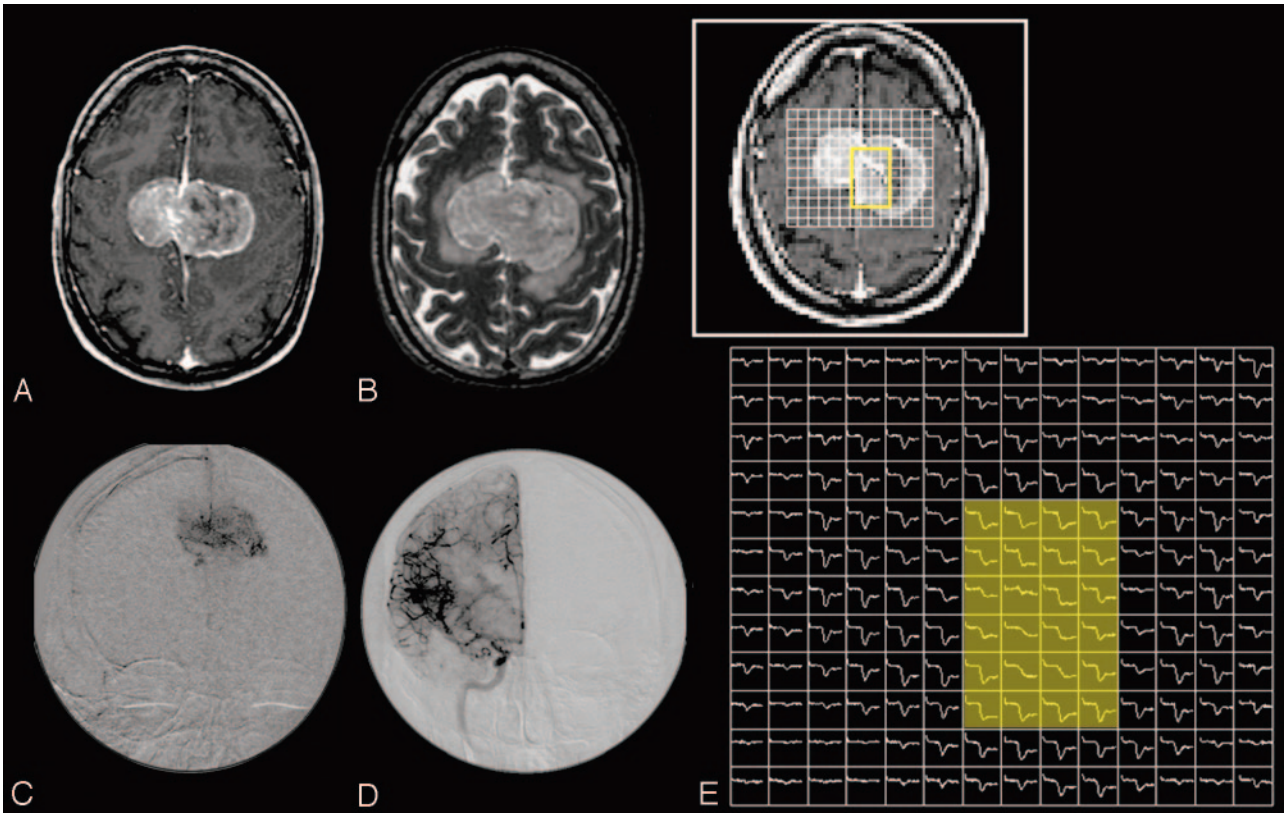

Fig 8. A 42-year-old man with bifalcine meningioma.

A and *B,* Axial postcontrast T1-weighted (*A*) and T2-weighted (*B*) images show a large enhancing, bifalcine, extra-axial mass.

C and *D,* Catheter angiographic images from selective external carotid artery (*C*) and internal carotid artery (*D*) demonstrate abnormal tumor vascularity. The central aspect of the tumor appears to be supplied predominantly by the external carotid artery.

E, 2D array of susceptibility-weighted signal intensity time curve over the tumor shows different patterns of signal intensity recovery. The central region of the tumor (*yellow shaded area*), which is supplied by the external carotid artery, has markedly lower degree of signal intensity recovery than the tumor periphery supplied by the internal carotid artery.

phoma cells tend to center around preexistent brain vessels. DSC perfusion MR imaging alone, however, will not provide confident diagnostic differentiation between PCL and other types of malignant brain tumor. As noted above, DWI may provide further specificity because PCL tends to demonstrate reduced diffusion presumably due to high cellularity of the tumor.

Metastatic brain tumors usually do not pose a diagnostic dilemma on MR imaging, because they tend to be multiple, they are located near the gray matter–white matter junction or the subarachnoid space, and often a known history of systemic malignancy is present. Approximately 30% or more of metastatic brain tumors, however, can manifest as a single lesion in the brain and, in some cases, as the initial clinical presentation of systemic malignancy.[65] Common to all metastatic brain tumors is that their tumor capillaries do not resemble those of the brain but of the organ where the systemic cancer arose.[66] Because the capillaries outside the brain do not possess the unique barrier function of the brain capillaries, metastatic brain tumors contain capillaries that are highly leaky. This is

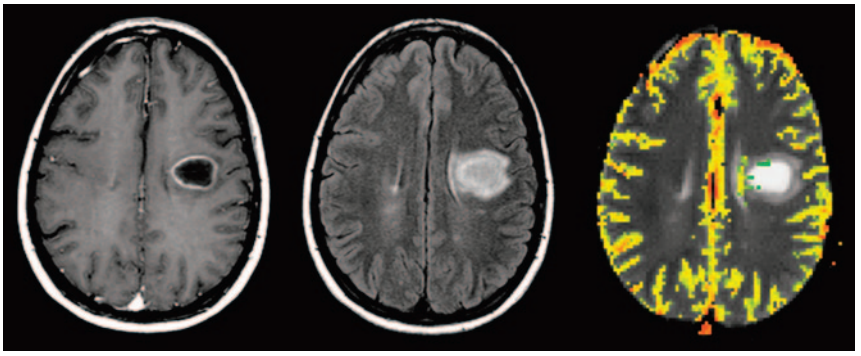

Fig 9. A 31-year-old woman with left frontal lobe tumefactive demyelinating lesion. Axial postcontrast T1-weighted (*left*) and FLAIR (*middle*) images show a rim enhancing left frontal mass. Relative cerebral blood volume map demonstrates lack of increased in blood volume within the lesion.

reflected in the susceptibility-weighted signal intensity–time curve where, similar to choroid plexus tumors, profound leakage of Gd-DTPA is noted in the early bolus phase. DSC perfusion MR imaging has shown useful in differentiating peritumoral edema of primary gliomas and metastatic brain tumors, where rCBV measurements within the vasogenic edema of metastasis were significantly lower than those within the infiltrative edema of gliomas.[67] Another study suggests that DSC perfusion MR imaging may be helpful in the assessment of radiosurgically treated brain metastases where rCBV measurements at 6 weeks posttreatment were predictive of clinical outcome.[68]

rCBV and Tumor-Mimicking Brain Lesions. Numerous lesions of the brain can simulate brain tumor on anatomic images, such as radiation necrosis,[69] subacute or infarct,[70] demyelinating lesion,[71] and infectious or inflammatory lesions.[72] These lesions frequently demonstrate contrast enhancement on postcontrast T1-weighted images due to leakage of Gd-DTPA into the interstitial space through a disrupted BBB. One of the prototypic non-neoplastic brain lesions often misdiagnosed as brain tumor is a tumefactive demyelinating lesion. These are large demyelinating lesions that can mimic high-grade glial tumors. Histopathologically, tumefactive demyelinating lesions consist of perivascular inflammatory infiltration and demyelination, but hypervascularity is uncommon.[73] On DSC perfusion MR images, tumefactive demyelinating lesions may demonstrate mild elevation of rCBV and characteristic intralesional venous enhancement, but marked hypervascularity is not seen (Fig 9).

DCE T1-Weighted Permeability Imaging

Endothelial permeability of vessels in brain tumors provides valuable information about BBB integrity, vascular morphology, and the nature of neovascularization, as well as tumor pathophysiology and prognosis.[73-76] Several recent studies have shown that quantitative estimates of microvascular permeability correlate with brain tumor grade.[73,77-79] Current and potential clinical uses for a noninvasive method to characterize microvascular permeability in brain tumors include guiding a surgeon to the most malignant spot for biopsy, monitoring efficacy or serving as primary end points of novel chemotherapy such as antiangiogenic drugs, manipulating the BBB for improved drug delivery, and differentiating therapy-related necrosis from recurrent tumor.

DCE perfusion MR imaging consists of repeated imaging with a T1-weighted sequence and measuring the shape of the contrast agent concentration curve in blood plasma, referred to as the arterial input function, and a time course of accumulation of contrast agent in tissue from individual voxels to calculate the size of the extravascular extracellular space and endothelial transfer coefficient K^{trans}. The most widely applied and accepted MR standard to measure permeability is the DCE steady-state T1-weighted method, which is based on the pharmacokinetic model of Tofts and Kermode.[80] This method fits a triexponential enhancement curve to a theoretic model based on compartmental analysis after injection of a single dose of Gd-DTPA. The mathematic pharmacokinetic compartmental modeling enables the concentration of Gd-DTPA in tissue to be calculated as a function of time after bolus injection of the contrast agent. The driving parameters in this model are the permeability surface area product of the endothelium (PS), the fractional size of the extravascular extracellular space (ve), the dose of injected Gd-DTPA, and the time course of blood plasma Gd-DTPA concentration or the arterial input function. A second model is used to relate the MR signal intensity to the Gd-DTPA concentration, where the 2 chief relationships to be considered are between (1) T1 and Gd-DTPA concentration and (2) MR signal intensity and T1. The relationship between T1 and Gd-DTPA concentration is approached by an in vitro value for relaxivity, and the intravascular contrast agent is ignored. Determination of how MR signal intensity will depend on T1 requires the knowledge of pre-enhancement T1 (ie, the T1 of the tissue before injection of gadopentetate dimeglumine) to calculate signal intensity enhancement. The complex modeling results in PS and ve, which characterize the biologic situation and, in theory, are independent of specific factors related to MR acquisition such as the particular sequence, injection rate, or type of MR system. DCE MR imaging also provides other simpler parameters—such as initial slope, time to peak, initial area under the contrast agent concentration–time curve—that characterize Gd-DTPA enhancement behavior. These simpler parameters are, however, subject to variability because of differences in MR acquisition, and their biologic representation is not clear.

The most widely used DCE MR imaging quantitative parameter is K^{trans}. The transfer constant K^{trans} is a generalized measure to describe the relationship between the time course of blood plasma Gd-DTPA concentration or the arterial input function and Gd-DTPA concentration changes occurring in the voxel. The PS of Gd-DTPA in abnormal brain tissue may

be limited by either the blood flow or the permeability. In brain tumors, the uptake of Gd-DTPA by tumor tissue is likely to be flow-limited because of abnormal vasculature that limits sufficient maintenance of the local plasma concentration at the arterial level. Regardless of the biologic situation, however, the mathematic analysis of the 2 situations has shown that shape and amplitude of the Gd-DTPA uptake curve can be identical for each and cannot distinguish between the 2. The transfer constant K^{trans} therefore is used in place of PS to describe either situation. K^{trans} is affected by several hemodynamic factors such as blood flow, blood volume, endothelial permeability, and endothelial permeability surface area, and the individual contribution of each component is difficult to measure. The Tofts model has since undergone analytic scrutiny and modeling refinements by numerous other investigators, which resulted in a more complex pharmacokinetic model to estimate individual hemodynamic components that alter K^{trans}. The basic principles of compartmental pharmacokinetics and mathematic modeling involved in DCE MR imaging are beyond the scope of this review, and interested readers are referred to several excellent review articles on this topic.[81-83]

In brain tumors, the blood flow to the tumor tissue is often hampered by an abnormal tumor vasculature comprising immature or defective endothelium, tortuosity, and thrombosis. Hence, the uptake of Gd-DTPA by tumor tissue is mainly limited by blood flow, not by permeability; however, in inflammatory lesions such as a multiple sclerosis plaque, the limiting factor for tissue uptake of Gd-DTPA is permeability and not blood flow. It should be remembered that, in addition to the complexity of pharmacokinetic modeling, the inherent heterogeneity of brain tumor tissue and its vasculature further poses a significant challenge in permeability measurements and accurate interpretation of the data. The transfer constant K^{trans} derived from DCE MR imaging has been applied in many clinical settings and was shown to be useful in assessing the different stages of demyelinating plaques,[84] glioma grade,[85] and treatment response.[86,87] There is a clear advantage to using DCE MR imaging rather than DSC MR imaging: DCE MR imaging offers better spatial resolution, is resistant to susceptibility artifact, and allows reasonable imaging time. Results of a recently published report suggest, however, uncertainty in the analysis of a DCE dataset where the use of commonly accepted models led to systematic overestimation of K^{trans} and potentially large underestimates of the blood plasma volume fraction.[88] This raises the concern whether steady-state T1-weighted analysis methods with a modeling system specific to a certain tumor type can be generalized and applied to other brain tumor types. It is emphasized that both DSC and DCE MR imaging generate incredibly complex datasets, and calculation of hemodynamic variables based on many thousands of pixel signal intensity changes in brain tumors notorious for their geographic tissue heterogeneity remains a formidable challenge. Nevertheless, the transfer constant K^{trans} derived from DCE MR imaging and rCBV derived from DSC MR imaging remain the primary variables used by many investigators to represent altered capillary permeability and tumor angiogenesis, respectively.

K^{trans} and Glioma Grade. In essence, K^{trans} is a quantitative measure of the degree of increase in T1 due to accumulation of Gd-DTPA in tissue. Because higher-grade gliomas tend to demonstrate T1 enhancement after administration of Gd-DTPA, it is not surprising to find that K^{trans} correlates strongly with glioma grade, as shown by several published reports.[77,89,90] A recent study also showed that CBV derived from DCE MR imaging showed a strong correlation with glioma grade.[89] The fractional blood volume and K^{trans} derived from DCE MR imaging have also been correlated with glioma grade and histologic proliferative marker, MIB-1 index, respectively.[85] With increasing glioma grade, there is higher likelihood of T1-weighted contrast enhancement of the tumor and hence increasing K^{trans}.

K^{trans} Derived from DCE versus DSC Perfusion MR Imaging. Although K^{trans} derived from DCE MR imaging is considered the reference standard, an alternative method by using DSC perfusion MR imaging has been proposed.[91] This new approach estimates both CBV and vascular transfer constant on the basis of fitting a model of plasma tracer concentration to a theoretic expression for total tissue concentration. The method yields CBV and transfer constant K^{trans} values that are in agreement with known physiology and CBV measurements that may be more accurate than traditional intravascular indicator dilution measurements in brain tumors with a severely damaged BBB. This method can be retrospectively applied to the large amount of existing T2*-weighted image data and can be applied to existing data collection protocols without the need to alter the sequence, though a reduction in flip angle is desirable.

K^{trans} and Clinical Trial End Points. With the increasing pace of novel drug therapies targeting tumor vasculature, there is a need to evaluate the effects of drugs on their therapeutic targets in vivo and to devise a more effective clinical trial strategy with noninvasive quantitative end points to assess success of therapy. To that end, DCE MR imaging has been proposed as a primary imaging method to assess antiangiogenic and antivascular therapeutic agents not only in brain but also in other solid organs. In 2002, a workshop in England led to consensus recommendations and guidelines by incorporating the views of a multidisciplinary panel of experts that included MR radiologists and scientists, pharmacologists, clinical trial scientists, and representatives of the pharmaceutical industry.[92] In these guidelines, there were 2 primary end points from DCE MR imaging—K^{trans} and initial area under the gadolinium concentration–time curve (IAUGC)—obtained on a voxel-by-voxel basis recommended for assessment of antiangiogenic and antivascular therapeutics by using DCE MR imaging. Both K^{trans} and IAUGC require calculation of instantaneous tumor contrast agent concentration, based on the change in T1 relaxivity because of contrast agent uptake ($\Delta R1$). The $\Delta R1$ measurement requires (1) an estimate of contrast agent relaxivity in tumor vasculature and tissues, (2) measurement of tumor T1 relaxation rate immediately before contrast agent uptake, (3) accurate T1 measurement method verified for all spatial locations, coils, and MR systems used, (4) cardiac output or arterial input function measurements, and (5) reproducible injection (ideally an MR-compatible power injector) of contrast agent. The significance and implication of these guidelines cannot be overstated because it is the first of its kind to put forth quantitative MR imaging as the

primary end point for clinical trials in a standardized and consensus format.

Conclusion

Neuroimaging of brain tumors has evolved from a purely anatomy-based discipline to one that incorporates morphologic abnormality with physiologic alterations in extracellular compartment kinetics, cellular metabolism, and hemodynamics. Tremendous progress and widespread clinical use of physiology-based MR imaging have become an essential part of the diagnostic armamentarium to diagnose, guide surgery, monitor therapy response, and predict prognosis of patients with brain tumor. The incorporation of physiologic MR imaging, such as DWI, proton MR spectroscopy, and perfusion-weighted MR imaging, as part of the mainstream clinical imaging protocol has empowered neuroradiologists to begin the process of combining radiology with biology in brain tumors to provide meaningful and clinically relevant end points and biomarkers for clinical trials and assessment of malignancy. Much work lies ahead, however, to validate and provide efficacy of these methods in improving diagnostic accuracy, affecting patient care, monitoring dynamic changes within brain tumor and normal brain during therapy, and establishing them as the arbiter of novel therapy that may one day prove cure of brain tumor a reality.

References

1. Nolte J. **Gross anatomy and general organization of the central nervous system.** In: *The human brain: an introduction to its functional anatomy.* 4th ed. St Louis: Mosby;1999:51–75
2. Daumas-Duport C, Beuvon F, Varlet P, et al. **[Gliomas: WHO and Sainte-Anne Hospital classifications].** *Ann Pathol* 2000;20:413–28
3. Bulakbasi N, Guvenc I, Onguru O, et al. **The added value of the apparent diffusion coefficient calculation to magnetic resonance imaging in the differentiation and grading of malignant brain tumors.** *J Comput Assist Tomogr* 2004; 28:735–46
4. Kitis O, Altay H, Calli C, et al. **Minimum apparent diffusion coefficients in the evaluation of brain tumors.** *Eur J Radiol* 2005;55:393–400
5. Kono K, Inoue Y, Nakayama K, et al. **The role of diffusion-weighted imaging in patients with brain tumors.** *AJNR Am J Neuroradiol* 2001;22:1081–88
6. Sugahara T, Korogi Y, Kochi M, et al. **Usefulness of diffusion-weighted MRI with echo-planar technique in the evaluation of cellularity in gliomas.** *J Magn Reson Imaging* 1999;9:53–60
7. Guo AC, Cummings TJ, Dash RC, et al. **Lymphomas and high-grade astrocytomas: comparison of water diffusibility and histologic characteristics.** *Radiology* 2002;224:177–83
8. Filippi CG, Edgar MA, Ulug AM, et al. **Appearance of meningiomas on diffusion-weighted images: correlating diffusion constants with histopathologic findings.** *AJNR Am J Neuroradiol* 2001;22:65–72
9. Smith JS, Cha S, Mayo MC, et al. **Serial diffusion-weighted magnetic resonance imaging in cases of glioma: distinguishing tumor recurrence from postresection injury.** *J Neurosurg* 2005;103:428–38
10. Klatzo I. **Presidental address: neuropathological aspects of brain edema.** *J Neuropathol Exp Neurol* 1967;26:1–14
11. Eis M, Els T, Hoehn-Berlage M, et al. **Quantitative diffusion MR imaging of cerebral tumor and edema.** *Acta Neurochir Suppl (Wien)* 1994;60:344–46
12. Pauleit D, Langen KJ, Floeth F, et al. **Can the apparent diffusion coefficient be used as a noninvasive parameter to distinguish tumor tissue from peritumoral tissue in cerebral gliomas?** *J Magn Reson Imaging* 2004;20:758–64
13. Lu S, Ahn D, Johnson G, Cha S. **Peritumoral diffusion tensor imaging of high-grade gliomas and metastatic brain tumors.** *AJNR Am J Neuroradiol* 2003;24: 937–41
14. Jellison BJ, Field AS, Medow J, et al. **Diffusion tensor imaging of cerebral white matter: a pictorial review of physics, fiber tract anatomy, and tumor imaging patterns.** *AJNR Am J Neuroradiol* 2004;25:356–69
15. Lu S, Ahn D, Johnson G, et al. **Diffusion-tensor MR imaging of intracranial neoplasia and associated peritumoral edema: introduction of the tumor infiltration index.** *Radiology* 2004;232:221–28
16. Roberts TP, Liu F, Kassner A, et al. **Fiber density index correlates with reduced fractional anisotropy in white matter of patients with glioblastoma.** *AJNR Am J Neuroradiol* 2005;26:2183–86
17. DaSilva AF, Tuch DS, Wiegell MR, et al. **A primer on diffusion tensor imaging of anatomical substructures.** *Neurosurg Focus* 2003;15:E4
18. Beaulieu C, Allen PS. **Determinants of anisotropic water diffusion in nerves.** *Magn Reson Med* 1994;31:394–400
19. Yu CS, Li KC, Xuan Y, et al. **Diffusion tensor tractography in patients with cerebral tumors: a helpful technique for neurosurgical planning and postoperative assessment.** *Eur J Radiol* 2005;56:197–204
20. Astrakas LG, Zurakowski D, Tzika AA, et al. **Noninvasive magnetic resonance spectroscopic imaging biomarkers to predict the clinical grade of pediatric brain tumors.** *Clin Cancer Res* 2004;10:8220–28
21. Fountas KN, Kapsalaki EZ, Vogel RL, et al. **Noninvasive histologic grading of solid astrocytomas using proton magnetic resonance spectroscopy.** *Stereotact Funct Neurosurg* 2004;82:90–97
22. Huang Y, Lisboa PJ, El-Deredy W. **Tumour grading from magnetic resonance spectroscopy: a comparison of feature extraction with variable selection.** *Stat Med* 2003;22:147–64
23. Lukas L, Devos A, Suykens JA, et al. **Brain tumor classification based on long echo proton MRS signals.** *Artif Intell Med* 2004;31:73–89
24. Herminghaus S, Dierks T, Pilatus U, et al. **Determination of histopathological tumor grade in neuroepithelial brain tumors by using spectral pattern analysis of in vivo spectroscopic data.** *J Neurosurg* 2003;98:74–81
25. Ando K, Ishikura R, Nagami Y, et al. [**Usefulness of Cho/Cr ratio in proton MR spectroscopy for differentiating residual/recurrent glioma from non-neoplastic lesions**]**.** *Nippon Igaku Hoshasen Gakkai Zasshi* 2004;64:121–26
26. Plotkin M, Eisenacher J, Bruhn H, et al. **123I-IMT SPECT and 1H MR-spectroscopy at 3.0 T in the differential diagnosis of recurrent or residual gliomas: a comparative study.** *J Neurooncol* 2004;70:49–58
27. Traber F, Block W, Flacke S, et al. [**1H-MR Spectroscopy of brain tumors in the course of radiation therapy: use of fast spectroscopic imaging and single-voxel spectroscopy for diagnosing recurrence**]**.** *Rofo* 2002;174:33–42
28. Burger P. **Malignant astrocytic neoplasms: classification, pathology, anatomy, and response to therapy.** *Semin Oncol* 1986;13:16–20
29. Chan AS, Leung SY, Wong MP, et al. **Expression of vascular endothelial growth factor and its receptors in the anaplastic progression of astrocytoma, oligodendroglioma, and ependymoma.** *Am J Surg Pathol* 1998;22:816–26
30. Plate KH, Mennel HD. **Vascular morphology and angiogenesis in glial tumors.** *Exp Toxicol Pathol* 1995;47:89–94
31. Semenza GL. **Hypoxia, clonal selection, and the role of HIF-1 in tumor progression.** *Crit Rev Biochem Mol Biol* 2000;35:71–103
32. Zagzag D, Friedlander DR, Margolis B, et al. **Molecular events implicated in brain tumor angiogenesis and invasion.** *Pediatr Neurosurg* 2000;33:49–55
33. Allen N. **Oxidative metabolism of brain tumors.** *Prog Exp Tumor Res* 1972;17: 192–209
34. Remy C, Fouilhe N, Barba I, et al. **Evidence that mobile lipids detected in rat brain glioma by 1H nuclear magnetic resonance correspond to lipid droplets.** *Cancer Res* 1997;57:407–14
35. Kuesel AC, Sutherland GR, Halliday W, et al. **1H MRS of high grade astrocytomas: mobile lipid accumulation in necrotic tissue.** *NMR in biomedicine* 1994;7:149–55
36. Kaminogo M, Ishimaru H, Morikawa M, et al. **Diagnostic potential of short echo time MR spectroscopy of gliomas with single-voxel and point-resolved spatially localized proton spectroscopy of brain.** *Neuroradiology* 2001;43: 353–63
37. Negendank WG, Sauter R, Brown TR, et al. **Proton magnetic resonance spectroscopy in patients with glial tumors: a multicenter study.** *J Neurosurg* 1996; 84:449–58
38. Cheng LL, Chang I-W, Louis DN, et al. **Correlation of high-resolution magic angle spinning proton magnetic resonance spectroscopy with histopathology of intact human brain tumor specimens.** *Cancer Res* 1998;58:1825–32
39. Star-Lack J, Spielman D, Adalsteinsson E, et al. **In vivo lactate editing with simultaneous detection of choline, creatine, NAA, and lipid singlets at 1.5 T using PRESS excitation with applications to the study of brain and head and neck tumors.** *J Magn Reson* 1998;133:243–54
40. Li X, Vigneron DB, Cha S, et al. **Relationship of MR-derived lactate, mobile lipids, and relative blood volume for gliomas in vivo.** *AJNR Am J Neuroradiol* 2005;26:760–69
41. Hoxworth JM, Cha S, Butowski N, et al. **Lactate-edited MRSI: Increased lactate in high grade gliomas prior to radiotherapy predicts treatment failure.** In: *Abstracts from the Society for Neuro-oncology Ninth Annual Meeting, Toronto* 2004:360
42. Plate KH, Risau W. **Angiogenesis in malignant gliomas.** *Glia* 1995;15:339–47
43. Wesseling P, Ruiter DJ, Burger PC. **Angiogenesis in brain tumors; pathobiological and clinical aspects.** *J Neurooncol* 1997;32:253–65
44. Zagzag D, Zhong H, Scalzitti JM, et al. **Expression of hypoxia-inducible factor 1alpha in brain tumors: association with angiogenesis, invasion, and progression.** *Cancer* 2000;88:2606–18
45. Puduvalli VK, Sawaya R. **Antiangiogenesis: therapeutic strategies and clinical implications for brain tumors.** *J Neurooncol* 2000;50:189–200
46. Zierler KL. **Theoretical basis of indicator-dilution methods for measuring flow and volume.** *Circ Res* 1962;10:393–407

47. Rosen BR, Belliveau JW, Vevea JM, et al. **Perfusion imaging with NMR contrast agents.** *Magn Res Med* 1990;14:249–65
48. Weisskoff R, Belliveau J, Kwong K, et al. **Functional MR imaging of capillary hemodynamics.** In: Potchen E, ed. *Magnetic resonance angiography: concepts and applications.* St Louis: Mosby;1993:473–84
49. Henry RG, Vigneron DB, Fischbein NJ, et al. **Comparison of relative cerebral blood volume and proton spectroscopy in patients with treated gliomas.** *AJNR Am J Neuroradiol* 2000;21:357–66
50. Cha S, Knopp EA, Johnson G, et al. **Intracranial mass lesions: dynamic contrast-enhanced susceptibility-weighted echo-planar perfusion MR imaging.** *Radiology* 2002;223:11–29
51. Chan A, Nelson S. **Simplified gamma variate fitting of perfusion curves.** *IEEE Int Symp Biomed Imaging* 2004;1067–70
52. Chan A, Pirzkall A, Nelson S. **Analysis of serial changes in perfusion parameters for patients with recurrent high grade gliomas being treated with radiosurgery.** In: Intl Soc Magn Reson Med. Kyoto, Japan, 2004
53. Jackson A, Kassner A, Zhu XP, et al. **Reproducibility of T2* blood volume and vascular tortuosity maps in cerebral gliomas.** *J Magn Reson Imaging* 2001;14: 510–16
54. Jackson A, Kassner A, Annesley-Williams D, et al. **Abnormalities in the recirculation phase of contrast agent bolus passage in cerebral gliomas: comparison with relative blood volume and tumor grade.** *AJNR Am J Neuroradiol* 2002; 23:7–14
55. Knopp EA, Cha S, Johnson G, et al. **Glial neoplasms: dynamic contrast-enhanced T2*-weighted MR imaging.** *Radiology* 1999;211:791–98
56. Weisskoff RM, Boxerman JL, Sorensen AG, et al. **Simultaneous blood volume and permeability mapping using a single Gd-based contrast injection.** In: International Society for Magnetic Resonance in Medicine. San Francisco, 1994; 279
57. Lupo JM, Cha S, Chang SM, Nelson SJ. **Dynamic susceptibility-weighted perfusion imaging of high-grade gliomas: characterization of spatial heterogeneity.** *AJNR Am J Neuroradiol* 2005;26:1446–54
58. Aronen HJ, Gazit IE, Louis DN, et al. **Cerebral blood volume maps of gliomas: comparison with tumor grade and histologic findings.** *Radiology* 1994;191: 41–51
59. Knopp EA, Cha S, Johnson G, et al. **Glial neoplasms: dynamic contrast-enhanced T2*-weighted MR imaging.** *Radiology* 1999;211:791–98
60. Lev MH, Ozsunar Y, Henson JW, et al. **Glial tumor grading and outcome prediction using dynamic spin-echo MR susceptibility mapping compared with conventional contrast-enhanced MR: confounding effect of elevated rCBV of oligodendrogliomas.** *AJNR Am J Neuroradiol* 2004;25:214–21
61. Sugahara T, Korogi Y, Kochi M, et al. **Correlation of MR imaging-determined cerebral blood volume maps with histologic and angiographic determination of vascularity of gliomas.** *AJR Am J Roentgenol* 1998;171:1479–86
62. Cha S, Tihan T, Crawford F, et al. **Differentiation of low-grade oligodendrogliomas from low-grade astrocytomas by using quantitative blood-volume measurements derived from dynamic susceptibility contrast-enhanced MR imaging.** *AJNR Am J Neuroradiol* 2005;26:266–73
63. Cha S, Martin A, Weber O, et al. **Intravenous and intra-arterial bolus tracking perfusion MR imaging of meningiomas before and after embolization [abstract].** In: *Proceedings of the 43rd Annual Meeting of the American Society of Neuroradiology, Toronto, 2005*; *Neuro News,* presentation number NN3
64. Pollack IF, Lunsford LD, Flickinger JC, Dameshek HL. **Prognostic factors in the diagnosis and treatment of primary central nervous system lymphoma.** *Cancer* 1989;63:939–47
65. Posner JB. **Management of brain metastases.** *Rev Neurol* 1992;148:477–87
66. Long DM. **Capillary ultrastructure in human metastatic brain tumors.** *J Neurosurg* 1979;51:53–58
67. Law M, Cha S, Knopp EA, et al. **High-grade gliomas and solitary metastases: differentiation by using perfusion and proton spectroscopic MR imaging.** *Radiology* 2002;222:715–21
68. Essig M, Waschkies M, Wenz F, et al. **Assessment of brain metastases with dynamic susceptibility-weighted contrast-enhanced MR imaging: initial results.** *Radiology* 2003;228:193–99
69. Schwartz RB, Carvalho PA, Alexander ED, et al. **Radiation necrosis vs high-grade recurrent glioma: differentiation by using dual-isotope SPECT with 201TI and 99mTc-HMPAO.** *AJNR Am J Neuroradiol* 1991;12:1187–92
70. Morgenstern LB, Frankowski RF. **Brain tumor masquerading as stroke.** *J Neurooncol* 1999;44:47–52
71. Zagzag D, Miller DC, Kleinman GM, et al. **Demyelinating disease versus tumor in surgical neuropathology: clues to a correct pathological diagnosis.** *Am J Surg Pathol* 1993;17:537–45
72. Ritter JH, Humphrey PA, Wick MR. **Malignant neoplasms capable of simulating inflammatory (myofibroblastic) pseudotumors and tumefactive fibroinflammatory lesions: pseudopseudotumors.** *Semin Diagn Pathol* 1998;15: 111–32
73. Provenzale JM, Wang GR, Brenner T, et al. **Comparison of permeability in high-grade and low-grade brain tumors using dynamic susceptibility contrast MR imaging.** *AJR Am J Roentgenol* 2002;178:711–16
74. Stewart PA, Hayakawa K, Farrell CL, et al. **Quantitative study of microvessel ultrastructure in human peritumoral brain tissue: evidence for a blood-brain barrier defect.** *J Neurosurg* 1987;67:697–705
75. Uematsu H, Maeda M, Sadato N, et al. **Vascular permeability: quantitative measurement with double-echo dynamic MR imaging: theory and clinical application.** *Radiology* 2000;214:912–17
76. Yang S, Law M, Zagzag D, et al. **Dynamic contrast-enhanced perfusion MR imaging measurements of endothelial permeability: differentiation between atypical and typical meningiomas.** *AJNR Am J Neuroradiol* 2003;24:1554–59
77. Roberts HC, Roberts TP, Brasch RC, et al. **Quantitative measurement of microvascular permeability in human brain tumors achieved using dynamic contrast-enhanced MR imaging: correlation with histologic grade.** *AJNR Am J Neuroradiol* 2000;21:891–99
78. Law M, Yang S, Babb JS, et al. **Comparison of cerebral blood volume and vascular permeability from dynamic susceptibility contrast-enhanced perfusion MR imaging with glioma grade.** *AJNR Am J Neuroradiol* 2004;25:746–55
79. Roberts HC, Roberts TP, Ley S, et al. **Quantitative estimation of microvascular permeability in human brain tumors: correlation of dynamic Gd-DTPA-enhanced MR imaging with histopathologic grading.** *Acad Radiol* 2002;9(suppl 1):S151–55
80. Tofts PS, Kermode AG. **Measurement of the blood-brain barrier permeability and leakage space using dynamic MR imaging. 1. Fundamental concepts.** *Magn Reson Med* 1991;17:357–67
81. Choyke PL, Dwyer AJ, Knopp MV. **Functional tumor imaging with dynamic contrast-enhanced magnetic resonance imaging.** *J Magn Reson Imaging* 2003; 17:509–20
82. Evelhoch JL. **Key factors in the acquisition of contrast kinetic data for oncology.** *J Magn Reson Imaging* 1999;10:254–59
83. Taylor JS, Tofts PS, Port R, et al. **MR imaging of tumor microcirculation: promise for the new millennium.** *J Magn Reson Imaging* 1999;10:903–07
84. Tofts PS, Barker GJ, Filippi M, et al. **An oblique cylinder contrast-adjusted (OCCA) phantom to measure the accuracy of MRI brain lesion volume estimation schemes in multiple sclerosis.** *Magn Reson Imaging* 1997;15:183–92
85. Roberts HC, Roberts TP, Bollen AW, et al. **Correlation of microvascular permeability derived from dynamic contrast-enhanced MR imaging with histologic grade and tumor labeling index: a study in human brain tumors.** *Acad Radiol* 2001;8:384–91
86. George ML, Dzik-Jurasz AS, Padhani AR, et al. **Non-invasive methods of assessing angiogenesis and their value in predicting response to treatment in colorectal cancer.** *Br J Surg* 2001;88:1628–36
87. Knopp MV, Giesel FL, Marcos H, et al. **Dynamic contrast-enhanced magnetic resonance imaging in oncology.** *Top Magn Reson Imaging* 2001;12:301–08
88. Buckley DL. **Uncertainty in the analysis of tracer kinetics using dynamic contrast-enhanced T1-weighted MRI.** *Magn Reson Med* 2002;47:601–06
89. Patankar TF, Haroon HA, Mills SJ, et al. **Is volume transfer coefficient (K[trans]) related to histologic grade in human gliomas?** *AJNR Am J Neuroradiol* 2005;26:2455–65
90. Ludemann L, Grieger W, Wurm R, et al. **Comparison of dynamic contrast-enhanced MRI with WHO tumor grading for gliomas.** *Eur Radiol* 2001;11: 1231–41
91. Johnson G, Wetzel SG, Cha S, et al. **Measuring blood volume and vascular transfer constant from dynamic, T(2)*-weighted contrast-enhanced MRI.** *Magn Reson Med* 2004;51:961–68
92. Leach MO, Brindle KM, Evelhoch JL, et al. **Assessment of antiangiogenic and antivascular therapeutics using MRI: recommendations for appropriate methodology for clinical trials.** *Br J Radiol* 2003;76:S87–91